Readout of a 176 pixel FDM system for SAFARI TES arrays

Hijmering, R. A.; den Hartog, R; Ridder, M.; Van Der Linden, A. J.; Van Der Kuur, J.; Gao, J. R.; Jackson, B.

Citation (APA)
Hijmering, R. A., den Hartog, R., Ridder, M., Van Der Linden, A. J., Van Der Kuur, J., Gao, J. R., & Jackson, B. (2016). Readout of a 176 pixel FDM system for SAFARI TES arrays. In J. Zmuidzinas, & W. S. Holland (Eds.), *Proceedings of SPIE: Millimeter, Submillimeter, and Far-Infrared Detectors and Instrumentation for Astronomy VIII* (Vol. 9914). Article 99141C SPIE. https://doi.org/10.1117/12.2231714

Important note
To cite this publication, please use the final published version (if applicable).
Please check the document version above.

Readout of a 176 pixel FDM system for SAFARI TES arrays

R. A. Hijmering, R. den Hartog, M. Ridder, A. J. van der
Linden, J. van der Kuur, et al.

SPIE.

Readout of a 176 pixel FDM system for SAFARI TES arrays

R. A. Hijmering[a], R. den Hartog[a], M. Ridder[a], A.J. van der Linden[a], J. van der Kuur[a], J. R. Gao[a,b], B. Jackson[c]

[a] SRON Netherlands Institute for Space Research, Utrecht, The Netherlands
[b] Kavli Institute of NanoScience, Delft University of Technology, Delft, the Netherlands
[c] SRON Netherlands Institute for Space Research, Groningen, The Netherlands

ABSTRACT

In this paper we present the results of our 176-pixel prototype of the FDM readout system for SAFARI, a TES-based focal-plane instrument for the far-IR SPICA mission. We have implemented the knowledge obtained from the detailed study on electrical crosstalk reported previously. The effect of carrier leakage is reduced by a factor two, mutual impedance is reduced to below 1 nH and mutual inductance is removed. The pixels are connected in stages, one quarter of the array half of the array and the full array, to resolve intermediate technical issues. A semi-automated procedure was incorporated to find all optimal settings for all pixels. And as a final step the complete array has been connected and 132 pixels have been read out simultaneously within the frequency range of 1-3.8MHz with an average frequency separation of 16kHz. The noise was found to be detector limited and was not affected by reading out all pixels in a FDM mode. With this result the concept of using FDM for multiplexed bolometer read out for the SAFARI instrument has been demonstrated.

Keywords: Readout, FDM,TES, bolometers, SPICA, SAFARI

1. INTRODUCTION

SAFARI[1],[2] is a grating spectrometer instrument for the Japanese/European far-IR SPICA mission proposed for the ESA M5 selection. It is based on three arrays with in total 3528 TES-based[3] bolometers with noise-equivalent powers (*NEP*) of 2×10^{-19} W/√Hz. The arrays will be operated in four wavelength bands: SW: 34-56 μm, MW: 54-89 μm, LW1: 87-143 μm, LW2: 140-230 μm, with background-limited sensitivity and high efficiency. SRON is developing Frequency Domain Multiplexing (FDM) for the read out of large AC biased TES arrays for both the SAFARI instrument, and the XIFU instrument on the X-ray Athena mission. FDM is already being used in several ground-based systems, e.g. for bolometer read-out for Cosmic Microwave Background observations[4],[5],[6]. In FDM for SAFARI, the TES bolometers are AC biased and readout using 24 channels. Each channel contains 160 pixels of which the resonance frequencies are defined by in-house developed cryogenic lithographic LC filters. FDM is based on the amplitude modulation of a carrier signal, which also provides the AC voltage bias, with the signal detected by the TES[7],[8]. To overcome the dynamic range limitations of the SQUID pre-amplifier baseband feedback (BBFB)[9],[10],[11] is applied. BBFB attempts to cancel the error signal in the sum-point, at the input of the SQUID, by feeding back a remodulated signal to the sum-point, and therefore improving the dynamic range of the SQUID pre-amplifier.

Previously we have reported on the successful low-noise read-out of 38 TES bolometer array[12],[13] and a detailed study on the effects of electrical crosstalk using our first iteration of a prototype of the full 160 pixel FDM experiment[14]. Using the obtained knowledge, a second generation prototype of a 176 pixel FDM experiment is developed in which the crosstalk due to carrier leakage, mutual inductance and common impedance are minimized. The cold part of the experiment consists of a detector chip with 176 pixels, which have a designed *NEP* of 7×10^{-19} W/√Hz, and two matching LC filter chips, each of which contains 88 carefully placed high-Q resonators, with in total 176 different resonance frequencies, and a single-stage SQUID. In this paper we present the initial experimental results of this successful 176 pixel FDM demonstration.

2. EXPERIMENTAL SET-UP

2.1 Warm electronics

In the FDM read out scheme[15] of which a schematic representation is shown in Figure 1, each TES is AC biased and is put in series with a LC filter with an unique resonance frequency. A comb of AC carriers is created by the DAC_{bias}, positioned on the DEMUX board at 300K, on a single line connected to the LC filters providing the bias signals for all TES detectors. Each LC filter filters out all carriers except one which biases the corresponding TES in its setpoint. After the TES detectors all signals are summed again and fed into a SQUID amplifier via the input coil. The amplified signal is fed via a low noise amplifier (LNA), located on the front end electronics (FEE) at 300K, into the ADC on the DEMUX board. On the DEMUX board the combined signals are demodulated to provide the *I* and *Q* signal of each pixel (TES+LC line). The demodulated signal is remodulated and sent, by the DAC_{fb}, back to the SQUID in order to provide the BBFB to overcome the limitations in dynamic rang of the SQUID amplifier. All components are built in house except for the SQUID amplifier which is provided by PTB (Germany) .
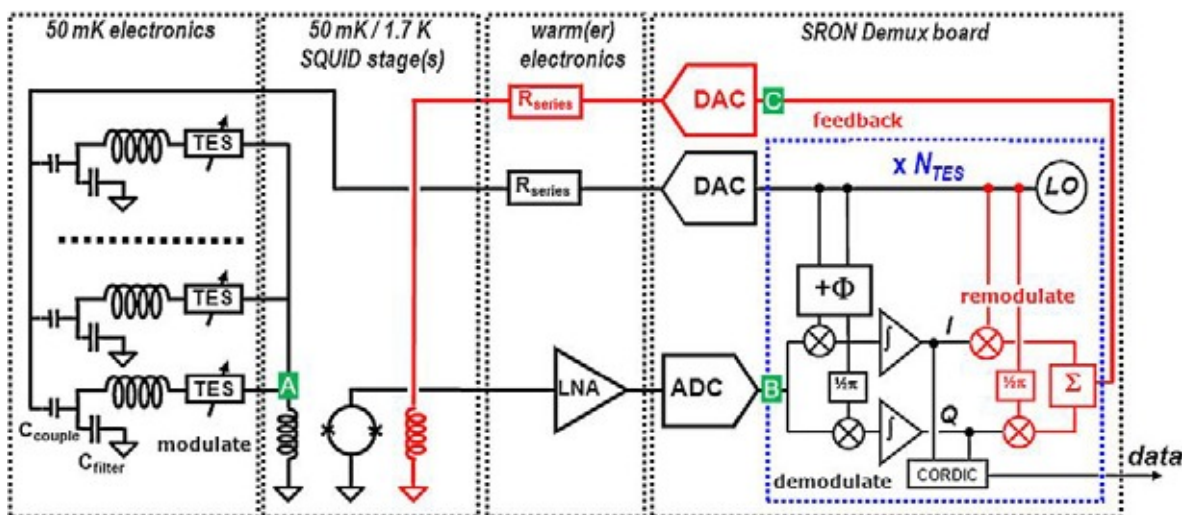

Figure 1. Schematic representation of the FDM bias and read out scheme.
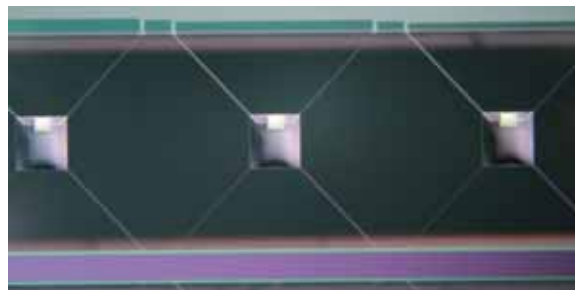
2.2 TES bolometer
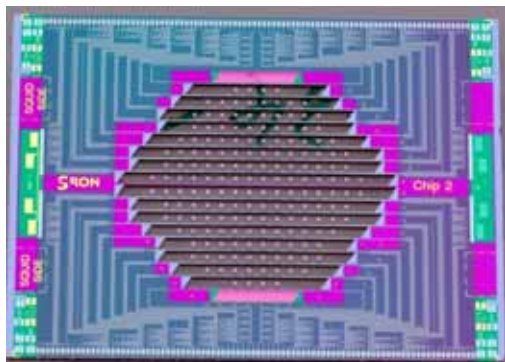
Figure 2 a) TES array containing 176 TES bolometers; b) a close up on some of the TES bolometers in the array.

The TES array contains 168 TES bolometers and 8 resistors, Figure 2 and is fabricated using the wet-etch procedure to remove the Si substrate in order to form the SiN supporting and thermal isolation structures[16]. The resistors, which have

a design resistance of 30 mΩ, which are equally spread out in position over the array and in frequency, are used as anchor points in for mapping the measured resonance frequency to position on the LC filter and TES array.

The TES bolometers are 50×50μm² Ti/Au, with thicknesses of 16 and 65 nm, a critical temperature (T_c) of 105 mK and normal resistance of 180 mΩ. They are situated, together with a 100×100 μm² Ta absorber with a thickness of 7 nm, on a 200×200 μm² SiN island which has a thickness of 500 nm. The 4 SiN legs that run from the island to the Si bars, and therefore transport the heat from the TES to the bath, are 2 μm wide, 400 μm long and have the same thickness as the island. The design value for the *NEP* of the TES bolometers is 7×10^{-19} W/√Hz, which is above the SAFARI requirement in order to assure they can be characterized in the 65 mK environment of the dry Janis adiabatic demagnetization refrigerator (ADR) at SRON. The design value of the saturation power is 20 fW. The TES array is patterned in a circle to fit within the radius of the used magnetic coil which is integrated in the experiment bracket.

The TES array is made to be symmetric, which simplifies the design process and makes the geometry more efficient. With this simplified design it was possible to drastically shorten the leads to the TES bolometers and therefore reduce the effect on the resonance frequency due to added inductance by the wiring. Extra structures are present to equalize the wire length for all TES bolometers and with it the added inductance and shift in resonance frequency.

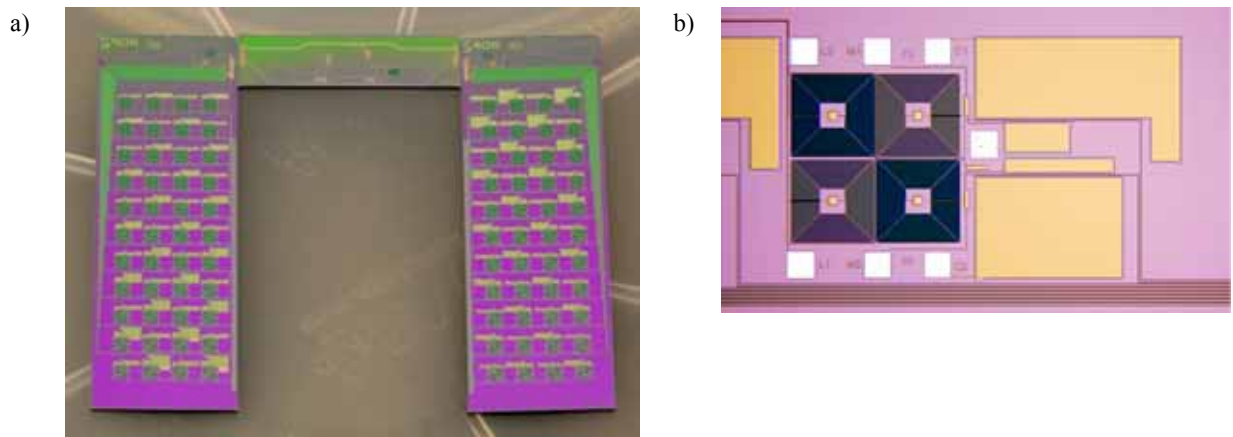### 2.3 LC filters

a) b)

Figure 3 Two LC filters used for the 176 pixel FDM experiment.

The LC filters[17] are spread out over two LC filter chips, as shown in Figure **3**a, with 88 LC filters per chip. All the wiring on the LC filter chips is based on μ-stripline to minimize the common inductance and influence on the resonance frequency due to added inductance by the wiring. The bias line enters on a central chip (named the SQUID fan out) and splits to the two LC filter chips. On the each LC filter chip the bias line is split into one line per unit cell which run on the outside of the LC chip. Each unit cell contains two LC filters (Figure **3**b) which are always more than 1 MHz apart in resonance frequency, again to minimize the effect of mutual inductance. Each LC filter is connected to the wiring for a TES on the TES chip using wirebonding. The return lines from the TES bolometers run on the outside of the LC filter as well to be summed again at the top close to the SQUID fan out chip. The summed signal line runs, via wirebonds, to the input coil of the SQUID which is glued on the SQUID fan out chip.

The resonance frequency of the LC filters ranges from 1 to 3.8 MHz. The coils of all LC filters are equal with a value of 3 μH and the capacitors, ranging from 0.5 to 8 nF, define the resonance frequency. The designed spacing between resonance frequencies is 16 kHz with a desired accuracy of ±1 kHz.
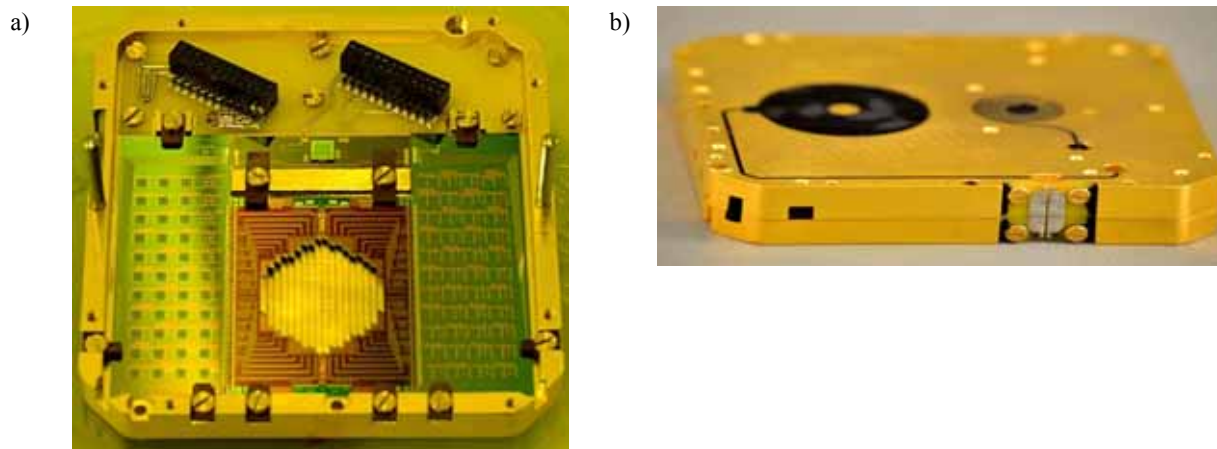
Figure 4 a) Assembled 176 pixel FDM experiment with SQUID fan out chip, LC filter chips and TES bolometer array; b) Same bracket but with the cover closed showing the integrated magnet and temperature sensor.

The LC filters alternate from one to the other LC filter chip to assure that LC filters with neighboring resonance frequencies are on different chips to create a maximum distance between the LC filters. This counters the effect of mutual inductance between neighboring frequencies[18]. On one LC filter chip the LC filters are placed such that also second neighbors in frequency always have a LC filter in between them which has a largely different resonance frequency but still accounts for a small slope in layer thickness across the wafer.

With this new design the mutual inductance between LC filters should become negligibly low. The common inductance is estimate to be 4.5 nH and consist of mainly the input coil of the SQUID, 3 nH, and the wirebonds between the LC filter chip and SQUID fan out chip. Carrier leakage is a feature of the design values (inductance of the LC filter and frequency separation) and should be reduced by a factor 2 compared to the previous 160 pixel FDM experiment[14].

The experiment is conducted in a ADR with a base temperature of 45 mK. To overcome the slowly increasing operating temperature, it is stabilized at 65 mK, which is still well below the T_c of 110 mK of the TES bolometers. The TES bolometers and LC filters are sensitive to magnetic fields[19] therefore the experimental environment is enclosed by a μ-metal shield to expel any remnant magnetic field. The sample bracket is situated inside a light tight box from which the gas can be evacuated via a light labyrinth coated with light absorbing material.

3. OBTAINING THE OPTIMAL PIXEL SETTINGS

With this large number of pixels a dedicated semi-automated procedure to obtain the optimal pixel settings for all pixels is imperative. In order to make finding the optimal settings manageable the following procedure is incorporated.
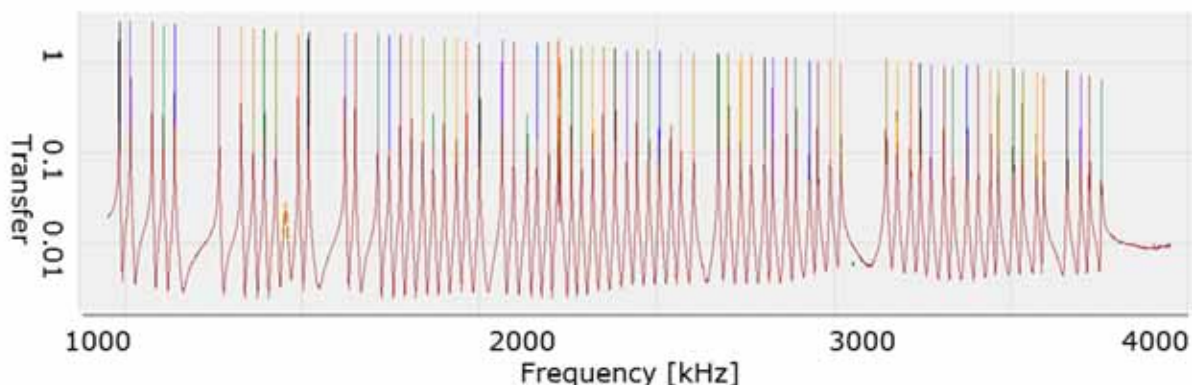

Figure 5 Example of a NWA scan via the bias line. Initially a rough scan use performed, to estimate the resonance frequencies, followed by individual detailed scans around the found frequencies.

At first a rough network analyzer (NWA) scan is performed via the bias line. This will give the first estimation of the resonance frequency ($f_{0,bias}$) via the bias line. The rough estimates are used as an input to perform detailed NWA scan around the resonance frequencies. These detailed scans will give the quality factor (Q) and the parasitic resistance (R_{par}) of the LC filters given by Equation **1** and Equation **2** resp.

$$Q = \Delta f_{0,bias} \Big/ f_{0,bias} \qquad \qquad \text{Equation 1}$$

$$R_{par} = \frac{1}{Q} \sqrt{L/C} \qquad \qquad \text{Equation 2}$$
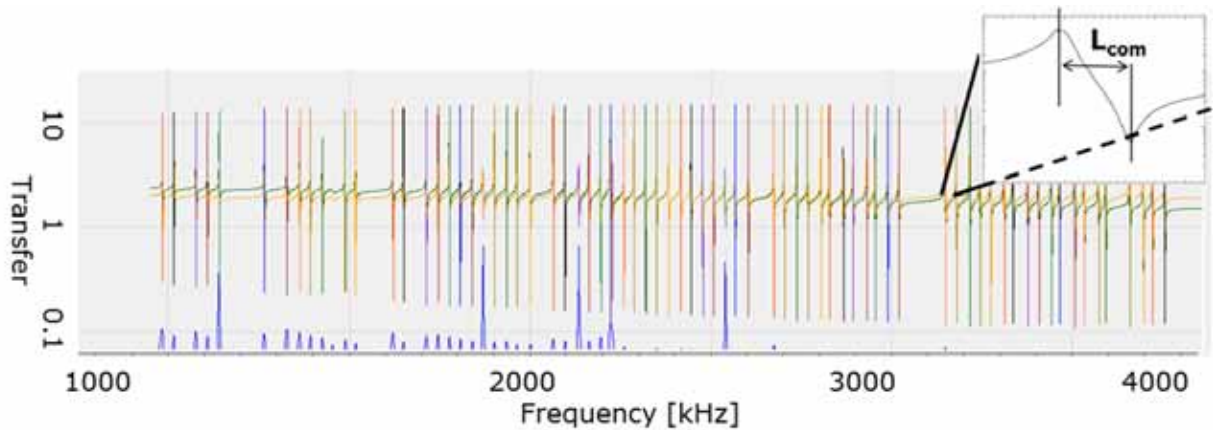

Figure 6 Example of a NWA scan via the feedback line. Initially a rough scan is performed to estimate the resonance frequencies, followed by individual detailed scans around the detected frequencies.

The same is performed via the feedback line to obtain the open loop resonance frequencies ($f_{0,OL}$) and the common inductance. The peak at the resonance frequency is determined by the LC-filter inductor, plus the common inductor, while the valley is determined by the LC filter alone. The difference of the two resonances gives the common inductance:

$$L_{com} = L \left[\left(\frac{f_{0,OL}}{f_{0,OL} - \Delta f} \right)^2 - 1 \right] \qquad \qquad \text{Equation 3}$$
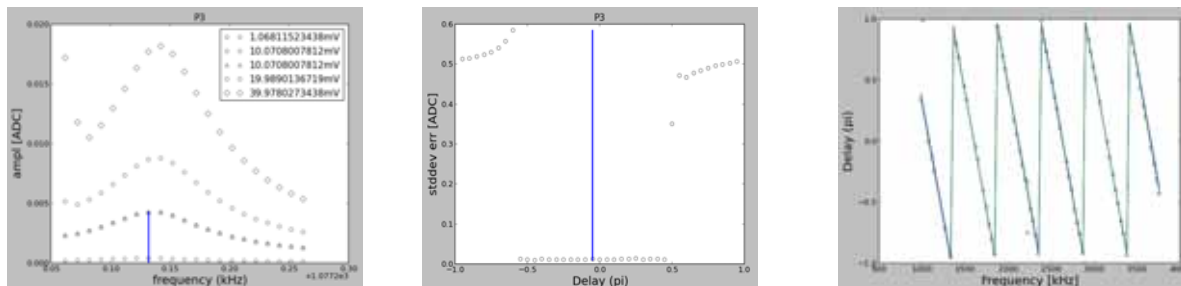

Figure 7 Example of a closed loop frequency scan, delay setting scan and resulting delay and resonance frequency settings with delay dependency fitted to the points.

When closing the BBFB loop part of the common inductance is screened by the feedback and the resonance frequency in closed loop is different from the resonance frequency in open loop. Thus a frequency scan in closed loop is needed to obtain the correct frequency. However, in order to close the loop the correct delay setting is needed at the frequency used. Therefor a delay scan, which determines the optimal delay setting at a frequency, and a closed loop frequency scan, to determine the closed loop resonance frequency ($f_{0,CL}$) are used iteratively. Examples of such results from these scans are shown in Figure 7.

With the delay and $f_{0,CL}$ settings known from IV curves, Figure 8, are taken to determine the set points for the pixels.
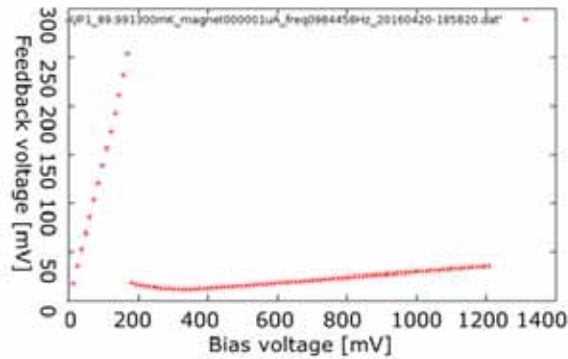

Figure 8. IV curve of one of the pixels to determine the setpoint in the transition of the TES

4. EXPERIMENTAL RESULTS

4.1 Circuit properties

In order to manage the complexity of the experiment a stepped approach is used. Firstly, a quarter of the total number of pixels (half of the left LC filter) is connected to perform initial tests on the system, followed by connecting half of the pixels, which is the complete left LC filter. In this configuration the frequency range is the same but the frequency spacing is double of the designed value (16 kHz) of the complete array. This 'simple' configuration is used to tackle issues faced during the experiment.
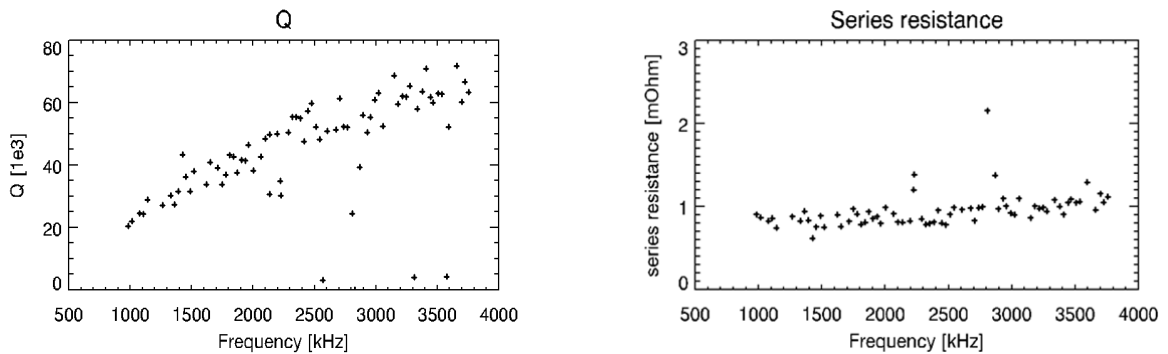

Figure 9a) Q values of the LC filters; b) parasitic resistance

Figure **9**a shows the quality values of the left LC filter chip, which range from 20.000 to 80.000, being well above the required 5.000. Figure **9**b shows the corresponding parasitic resistance, which is constant at a value of 1 mΩ.
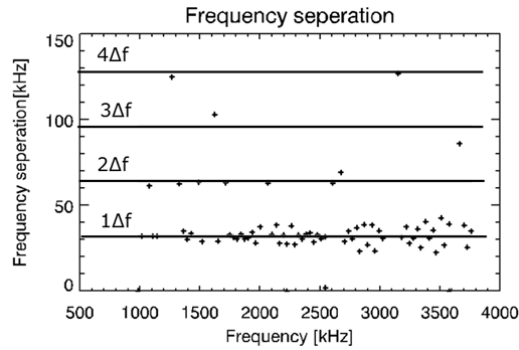
Figure 10. Frequency separation of the resonance frequencies on the left LC filter chip

Figure **10** shows the separation between the resonance frequencies. It is obvious the separation is well above the desired 1 kHz. During the previous 160 FDM experiment[14] some of the inductors from the LC filters showed shorts and thus result in large deviations in resonance frequency. In order to pin point any troublesome steps during production the wafers have been optical inspected after each production step. The extra handling of the wafers during production has consequences on the quality of the LC filters. However the required 1 kHz variation on the resonance frequency separation has been shown before by M. Bruijn *et al*[17].

4.2 Crosstalk
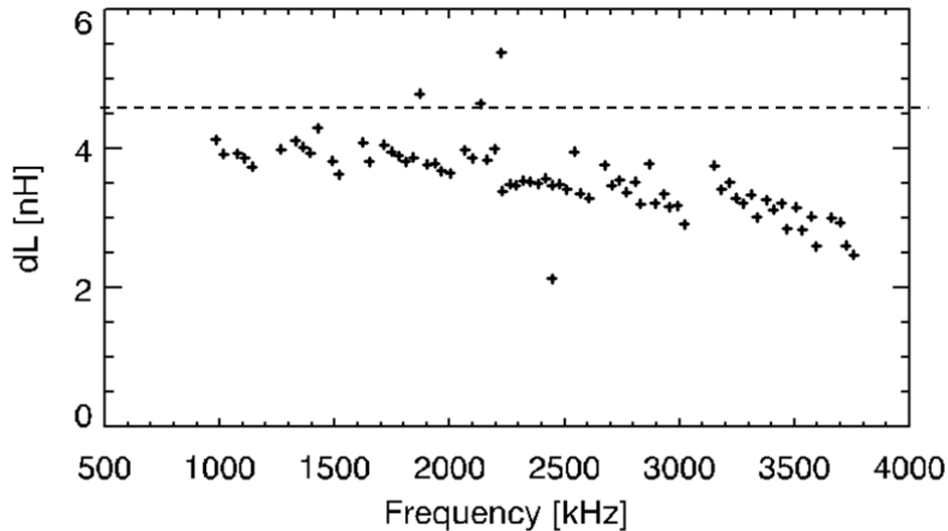
Figure 11 Common inductance as measured using the NWA scan via the feedback.

Figure **11** shows the measured common inductance resulting from the NWA scan via the feedback line. The measured common inductance is around 4 nH, which is slightly lower than the estimated 4.5 nH. The estimated value of 4.5 nH is obtained by 3 nH for the input coil of the SQUID and 1 nH for each wirebond. However, during mounting of the chips each connection between chips is produced using several wirebonds in parallel and therefor reducing their inductance explaining the lower measured common inductance.

Figure 12. a) schematic of the FDM circuit using the feedback on the feedback coil with the saturation powers as function of resonance frequency; b) Schematic of the FDM circuit using the feedback on the input coil, and therefore screening the common inductance, with the saturation powers as function of resonance frequency
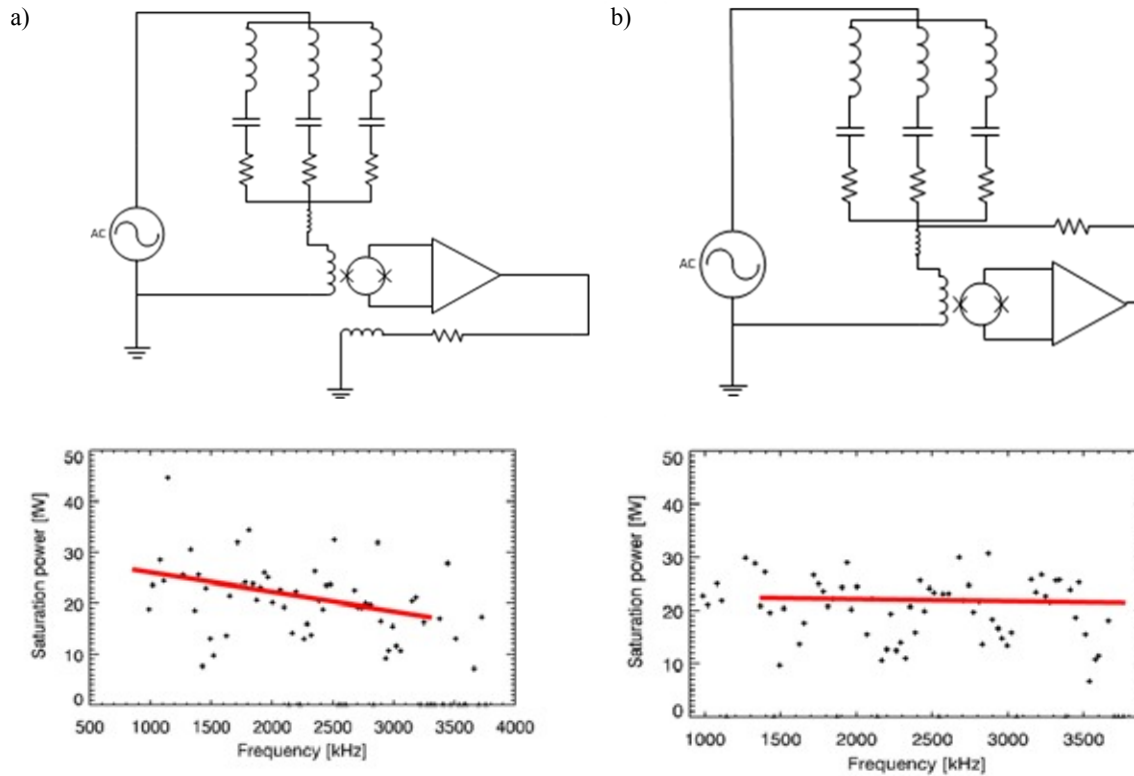
Figure **12**a shows the saturation power as a function of resonance frequency, measured with the initial FDM circuit. Evidently a slope is present in the saturation power as a function of resonance frequency caused by not taking into account the common inductance in the calibration. The circuit has been adapted by connecting the feedback to the input coil and therefor screening any inductance beyond this connection. The remaining common impedance outside the screened section is estimated to be well below 1 nH. The effect is clearly seen in the resulting measured saturation power as a function of resonance frequency in Figure **12**b. As also shown in Figure 13a the effect of the neighboring pixels in frequency on the saturation power is estimated to be below 7% and is mainly caused by carrier leakage, which is a property of the readout circuit. As a result, the IV curve shows a small effect on the normal branch when the nearest neighbors are switched on. Switching the second neighbors and further does not induce a notably additional effect.
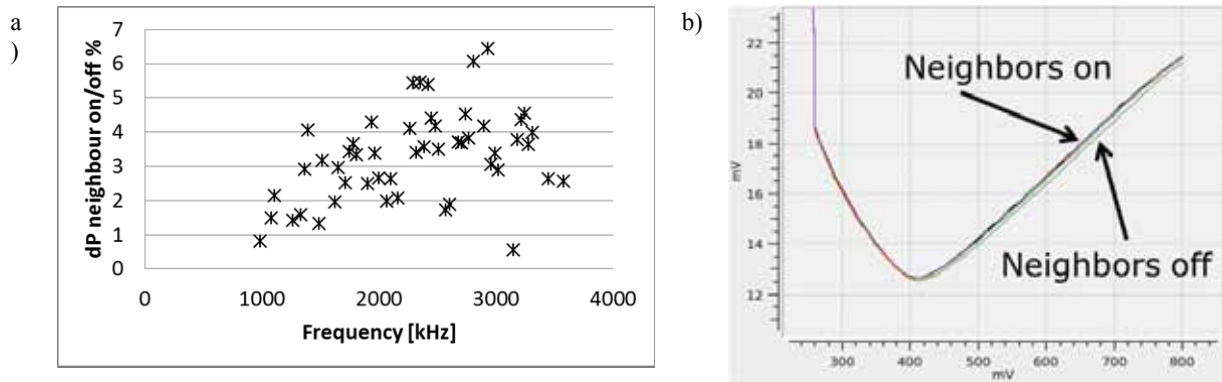
Figure 13 effect of switching neighboring frequency pixel on and off due to crosstalk.

4.3 Device properties

As shown in Figure **12**b the measured saturation power is close to the designed value of 20 fW. However, a large spread is present on the measured saturation power. This spread may be expected with the used wet-etching fabrication method because the process may cause a large variation of the G of the TES bolometers. There were also issues with the use of metal Cu deposition during the production of the resistors. A structure is present in the saturation power as a function of resonance frequency with a period of 500 kHz. Mapping the saturation powers on the TES array shows that the lower saturation powers are mainly located at the top region, while the higher saturation powers at the bottom part of the array. The period is caused by an overall slope in G across the TES array. This is verified by independent G measurements. This large variation in G with this array is not of concern since it is caused by the old fabrication method and has no influence on the demonstration of FDM. The new Deep-RIE fabrication method shows much improved fabrication accuracy, resulting therefore in more uniform G[19].

The noise of the devices is measured to be 6×10^{-19} W/√Hz, which agrees with the designed value of 7×10^{-19} W/√Hz. Both the saturation power and the *NEP* are close to the designed value, indicating that the system is well calibrated.
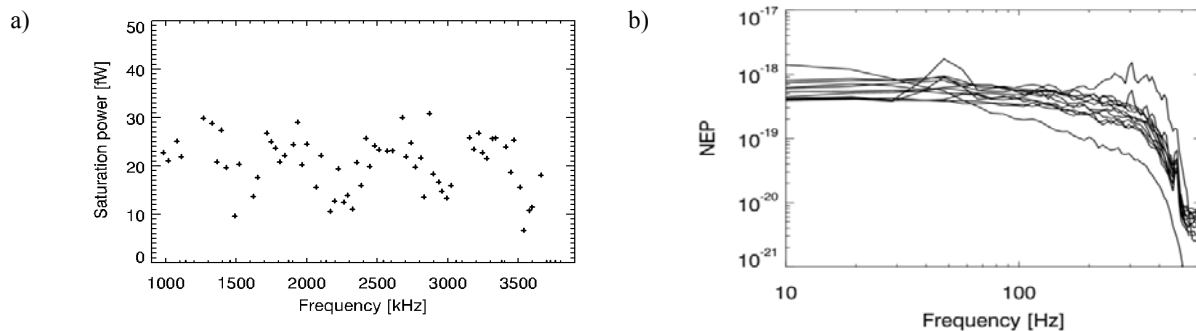

Figure 14 a) saturation power as function of resonance frequency and b) an example of the NEP of the TES bolometers.

After the very encouraging results with only the left LC filter chip connected, a further step was taken to connect the right LC filter chip. The variation on the frequency separation on this LC filter chip is 3 kHz, Figure **15**a, much better compared to the left LC filter chip. It must be mentioned that the LC filter chips are fabricated in pairs. Unfortunately for none of the LC filter chip pairs fabricated both LC filter chips where in working order. And although both LC filter chips are from the same wafer they are from a low and high quality position on the wafer and differences between the two LC filters are thus expected. The measured parasitic resistance for the right LC filter chip is larger compared to parasitic resistance as measured with the left LC filter chip. Before connecting the right LC filter chip a small repair job was conducted on the biasing circuit, which is the cause of this increased parasitic resistance and the measured parasitic resistance is not the parasitic resistance from the LC filters. Since the increased resistance on the bias line is still well below the value limiting stable biasing of the pixels it is of no influence on the FDM read out results.
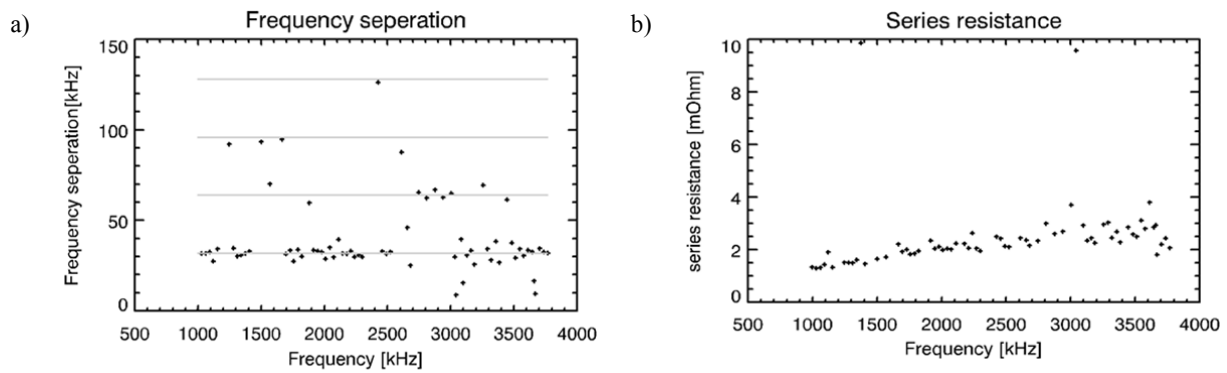
Figure 15. a) Frequency separation and; b) parasitic resistance of the right LC filter chip

4.4 Demonstration of FDM with 132pixels read out simultaneously

With both LC filters connected individually and checked both LC filter chips are connected simultaneously. From the tests with the individual LC filter chips the malfunctioning pixels, either the TES bolometer or LC filter, have been identified and are excluded for the FDM demonstration.
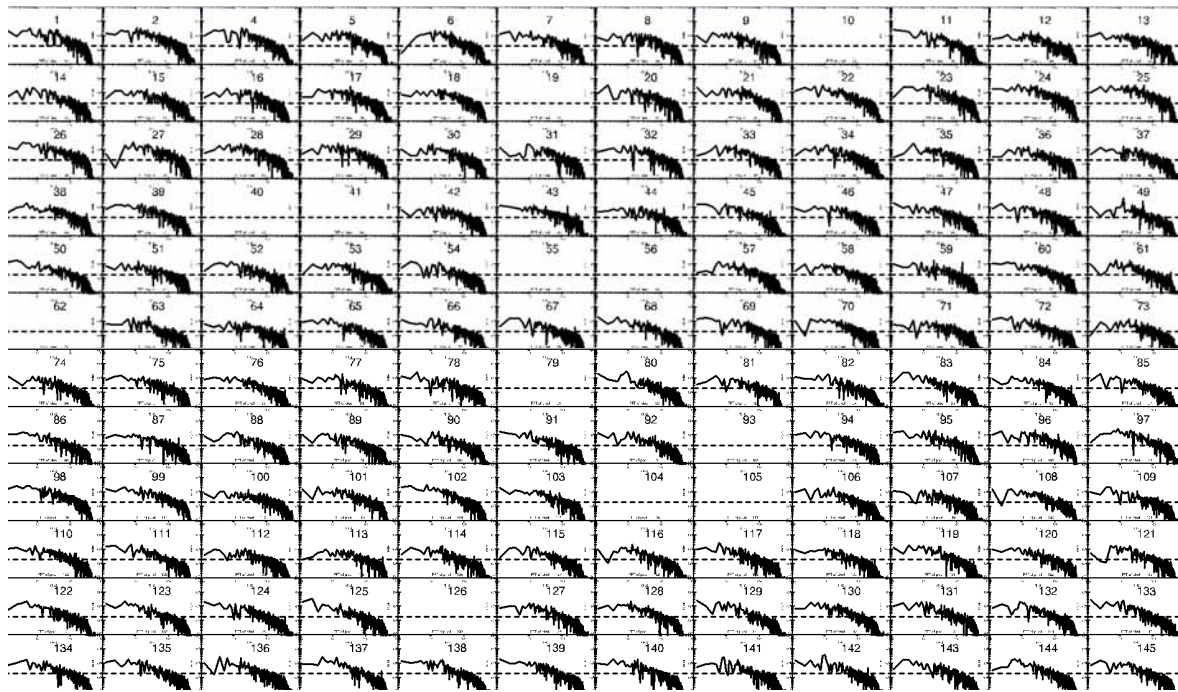

Figure 16 Noise measurement in FDM mode of 132 pixels. The scale of all plots is equal and the dashed line indicates the readout noise at the input of the SQUID.

Figure 16 shows the measured noise plots of 132 pixels, all of which are active and are read out simultaneously in FDM mode. The noise plots are produced by operating all TES bolometers in 50% of their transition and obtaining a data stream of 1s length in time and making a FFT to produce the noise plots. The scale of all plots is equal. The dashed lines indicate the readout noise, showing that the detector noise is above the readout noise. All pixels have the same gain bandwidth setting of ~600Hz. Empty plots are present, indicating those pixels were switched off. They are 8 resistors, 1 LC filter which had a connection to the other LC filter in its unit cell due to which they could not be biased simultaneously, 3 pixels which could not be biased, and one pixel is working order but which switched off by accident during the measurement.
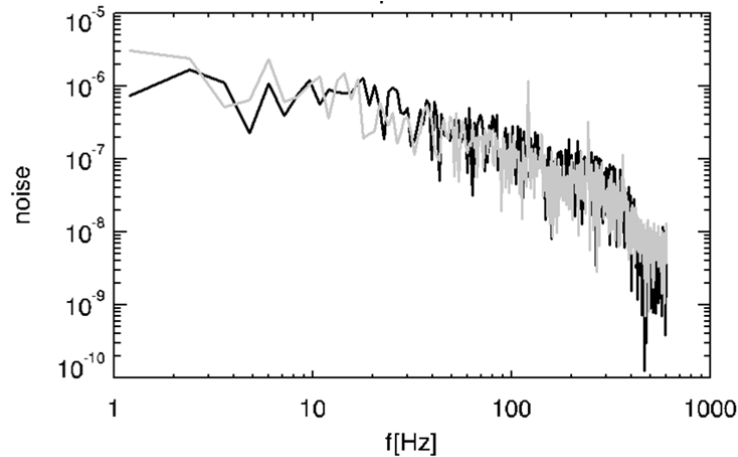
Figure 17 Example of a comparison of the measured noise with only a single pixel active (grey) and in FDM mode (black).

To show that the FDM readout does not noticeably affect the noise level Figure 17 shows a noise spectrum of a pixel in FDM mode and the noise spectrum of the same pixel with only that pixel switch on overplotted. As can be seen, there is no difference between the two noise spectra, illustrating that the FDM mode does not affect the noise level.

5. SUMMARY AND DISCUSSIONS

In this paper we have presented the initial results of the 176 pixel FDM experiment to demonstrate the working principle of the 160 pixel FDM proposed for the SAFARI instrument.

A procedure has been developed, to find the optimal settings for all the individual pixels. It starts with NWA scans via the bias line and feedback line to find the first estimated of the open loop resonance frequencies and properties of the resonance circuit as Q, parasitic resistance and common impedance. Close loop scans on each pixel are used in iterative fashion to determine the correct resonance frequency and delay settings. The procedure is tested and ready to be put into more permanent automated software.

A stepped approach is applied to connect the pixels to find problems in the set-up. Unfortunately it proved that both the TES array and LC filter chips where not of the high quality as desired for the final instrument. The spread on resonance frequency separation was larger and due to extra handling of the LC filter chips during fabrication for increased inspections. Large G variations are present in the TES array used, which is attributed to the wet-etching fabrication process. Additionally, issues were experienced with the Cu used for the resistors.

The electrical crosstalk in the system was mainly present in the form of common impedance initially. This was due to the 4nH impedance introduced by the wirebonds and input coil of the SQUID. By placing the feedback into the input coil of the SQUID including most of the wirebonds, the common impedance was screened out. The resulting effect was clearly seen in the results for the saturation power. The remaining crosstalk, of <7% on the saturation power, is due to the carrier leakage, which is inherit to the circuit design.

With both LC filter chips tested, they were connected and 132 pixels have been successfully read out simultaneously. The remaining pixels are either the resistors or the pixels that have problems either due to the TES or LC filter. All pixels were biased in the transition at 50% of the normal resistance. The measured TES current noise was well above the electronic noise. A comparison between the current noise in FDM mode and in single pixel mode shows no effect on the noise by applying the FDM mode. This result suggests that the 160 pixel FDM concept for the SAFARI instrument for the SPICA mission has been in principle demonstrated.

REFERENCES

[1] Jackson, B.D., Korte, P.A.J.de, van der Kuur, J., Mauskopf, P.D., Beyer, J., Bruijn, M.P., Cros, A., Gao, J.-R., Griffin, D., Hartog, R.den, Kiviranta, M., Lange, G.de, Leeuwen, B.-J.van, Macculi, C., Ravera, L., Trappe, N., Weers, H.van, Withington, S.,"The SPICA- SAFARI detector system: TES detector arrays with frequency-division multiplexed SQUID readout", IEEE Transactions on Terahertz Science and Technology 2 (99), 1–10, (2011)

[2] Roelfsema, P., Giard, M., Najarro, F., Wafelbakker, K., Jellema, W., Jackson, B., Sibthorpe, B., Audard, M., di Giorgio, A., Griffin, M., Helmich, F., Kamp, I., Kerschbaum, F., Meyer, M., Naylor , D., Onaka, T., Poglitch, A., Spinoglio , L., van der Tak , F., Vandenbussche, B.,"SAFARI new and improved: extending the capabilities of SPICA's imaging spectrometer", Proc. SPIE 9143, 91431K, (2014)

[3] K.D.Irwin , in Topics in Applied Physics: "Cryogenic particle detection", ed. by C.Enss, Berlin, Springer, (2005) Irwin, K.D., Hilton, G.C.,"", in Topics in Applied Physics: "Cryogenic particle detection", ed. by C.Enss, Berlin, Springer, (2005)

[4] Lanting, T. M., Cho, H. -M., Clarke, J., Holzapfel, W. L., Lee, A. T., Lueker, M., Richards, P. L. Dobbs, M.A, Spieler, H, Smith, A., "Frequency-domain multiplexed readout of transition-edge sensor arrays with a superconducting quantum interference device" Appl. Phys. Lett. **86**, 112511 (2005) Lanting, T., Cho, H., Clarke, J., Holzapfel, W., Lee, A., Lueker, M., Richards, P., Dobbs, M., Spieler, H., Smith, A.,"Frequency-domain multiplexed readout of transition-edge sensor arrays with a superconducting quantum interference device", Appl. Phys. Lett. 86, 112511, (2005)

[5] Lee, A.T.,"SQUID readout multiplexers for transition-edge sensor arrays", Proc. Nucl. Instr.and Meth. A 559, 786, (2006)

[6] Dobbs, M.A., Lueker, M., Aird, K.A., Bender, A.N., Benson, B.A., Bleem, L.E., Carlstrom, J.E., Chang, C.L., Cho, H.-M., Clarke, J., Crawford, T.M., Crites, A.T., Flanigan, D.I., Haan, T.de, George, E.M., Halverson, N.W., Holzapfel, W.L., Hrubes, J.D., Johnson, B.R., Joseph, J., Keisler, R., Kennedy, J., Kermish, Z., Lanting, T.M., Lee, A.T., Leitch, E.M., Luong-Van, D., McMahon, J.J., Mehl, J., Meyer, S.S., Montroy, T.E., Padin, S., Plagge, T., Pryke, C., Richards, P.L., Ruhl, J.E., Schaffer, K.K., Schwan, D., Shirokoff, E., Spieler, H.G., Staniszewski, Z., Stark, A.A., Vanderlinde, K., Vieira, J.D., Vu, C., Westbrook, B.,"Frequency Multiplexed SQUID Readout of Large Bolometer Arrays for Cosmic Microwave Background Measurements", Rev. Sci. Instrum. **83**, 073113, (2012) Dobbs, M.A., Lueker, M., Aird, K.A., Bender, A.N., Benson, B.A., Bleem, L.E., Carlstrom, J.E., Chang, C.L., Cho, H.-M., Clarke, J., Crawford, T.M., Crites, A.T., Flanigan, D.I., Haan, T.de, George, E.M., Halverson, N.W., Holzapfel, W.L., Hrubes, J.D., Johnson, B.R., Joseph, J., Keisler, R., Kennedy, J., Kermish, Z., Lanting, T.M., Lee, A.T., Leitch, E.M., Luong-Van, D., McMahon, J.J., Mehl, J., Meyer, S.S., Montroy, T.E., Padin, S., Plagge, T., Pryke, C., Richards, P.L., Ruhl, J.E., Schaffer, K.K., Schwan, D., Shirokoff, E., Spieler, H.G., Staniszewski, Z., Stark, A.A., Vanderlinde, K., Vieira, J.D., Vu, C., Westbrook, B., Williamson, R.,"Frequency Multiplexed SQUID Readout of Large Bolometer Arrays for Cosmic Microwave Background Measurements", Rev. Sci. Instrum. 83, 073113, (2012)

[7] Yoon, Jongsoo, Clarke, John, Gildemeister, J.M., Lee, AdrianT., Myers, M.J., Richards, P.L., Skidmore, J.T.,"Single superconducting quantum interference device multiplexer for arrays of low-temperature sensors", Appl. Phys. Lett. 78, 371, (2001)

[8] Kiviranta, M. *et al.*,"SQUID-based readout schemes for microcalorimeter arrays" AIP Conf. Proc. **605**, 295 (2002) Kivirantaa, Mikko, Heikki, , der, Janvan, Korte, Pietde,"SQUID-based Readout Schemes for Microcalorimeter Arrays", AIP Conf. Proc. 605, 295, (2002)

[9] Van der Kuur, J., Beyer, J., Boersma, D., Bruin, M., Gottardi, L., Hartog, R.den, Hoevers, H., Hou, R., Kiviranta, M., Korte, P.J.de, Leeuwen, B.?J.van,"Progress on Frequency-Domain Multiplexing Development for High Count rate X-ray Microcalorimeters", AIP Conf. Proc. 1185, 245, (2009)

[10] den Hartog, R., Boersma, D., Bruijn, M., Dirks, B., Gottardi, L., Hoevers, H., Hou, R., Kiviranta, M., de Korte, P., van der Kuur, J., van Leeuwen, B.?J., Nieuwenhuizen, A., Popescu, M.,"Baseband Feedback for Frequency-Domain-Multiplexed Readout of TES X-ray Detectors", AIP Conf. Proc. 1185, 261, (2009)

[11] Takei, Y., Yamasaki, N.Y., Hirakoso, W., Kimura, S., Mitsuda, K.,"SQUID multiplexing using baseband feedback for space application of transition-edge sensor microcalorimeters", Supercond. Sci. Technol. 22, 114008, (2009)

[12] den Hartog, R., Audley, M.D., Beyer, J., Boersma, D., Bruijn, M., Gottardi, L., Hoevers, H., Hou, R., Keizer, G., Khosropanah, P., Kiviranta, M., de Korte, P., van der Kuur, J., van Leeuwen, B.-J., Nieuwenhuizen, A.C.T., van Winden, P.,"Low-Noise Readout of TES Detectors with Baseband Feedback Frequency Domain Multiplexing", J. of Low Temp. Phys. 167, 652, (2012)

[13] den Hartog ,R. *et al.*," Low-Noise Readout of TES Detectors with Baseband Feedback Frequency Domain Multiplexing" J. of Low Temp. Phys. **167**, 652 (2012) den Hartog, R.H., Bruijn, M.P., Clenet, A., Gottardi, L., Hijmering, R., Jackson, B.D., van der Kuur, J., van Leeuwen, B.J., van der Linden, A.J., van Loon, D., Nieuwenhuizen, A., Ridder, M., van Winden, P.,"Progress on the FDM development at SRON: toward 160 pixels", J. of Low Temp. Phys. 170, 439, (2014)

[14] Hijmering, R.A., den Hartog, R.H., van der Linden, A.J., Ridder, M., Bruijn, M.P., van der Kuur, J., van Leeuwen, B.J., van Winden, P., Jackson, B.,"The 160 TES bolometer read-out using FDM for SAFARI", Proc. SPIE 91531E, (2014)

[15] Clénet, A., Ravera, L., Bertrand, B., Cros, A., Hou, R., Jackson, B.J., van Leeuwen, B.J., Van Loon, D., Parot, Y., Pointecouteau, E., Sournac, A., Ta, N.,"The DCU; the detector control unit for SPICA-SAFARI", Proc. SPIE, 914346, (2014)

[16] M.L. Ridder, P. Khosropanah, R.A. Hijmering, T. Suzuki, M.P. Bruijn, H.F.C. Hoevers, J.R. Gao, M.R. Zuiddam, "Fabrication of Low-Noise TES Arrays for the SAFARI Instrument on SPICA", J. Low. Temp. Phys. 184, 60–65 (2016). Ridder, M.L., Khosropanah, P., Hijmering, R.A., Suzuki, T., Bruijn, M.P., Hoevers, H.F.C., Gao, J.R., Zuiddam, M.R.,"Fabrication of Low-Noise TES Arrays for the SAFARI Instrument on SPICA", J. Low. Temp. Phys. 184, 60–65, (2016)

[17] Bruijn, M.P., Gottardi, L., den Hartog, R.H., van der Kuur, J., van der Linden,, A.J.,"Tailoring the High-Q LC Filter Arrays for Readout of Kilo-Pixel TES Arrays in the SPICA-SAFARI Instrument", J. of Low Temp. Phys. 176, 421, (2014)

[18] Yan, X., Bruijn, M.P., van Rantwijk, J.F., van Weers, H.J., Hijmering, R.A., van de Kuur, J., Gao, and J.R.,"Modeling inductances of wiring for a TES array read by FDM", IEEE Trans. on app. Sup., 25, 3, (2014)

[19] Hijmering, R.A., Khosropanah, P., Ridder, M., Lindeman, M., Gottardi, L., Bruijn, M., van der Kuur, J., de Korte, P., Gao, J.-R., Hoevers, H., Jackson, B.,"Effects of magnetic fields on highly sensitive TiAu TES bolometers", IEEE Trans. on app. Sup. 23 ,3, (2013)

[20] Khosropanah, P., Suzuki, T., Ridder, M.L., Hijmering, R.A., Akamatsu, H., Gottardi, L., Van der Kuur, J., Gao, J.-R., Jackson, B.D.,"Ultra-low Noise TES bolometer Arrays for SAFARI Instrument on SPICA Authors: P. Khosropanah, T. Suzuki, M.L. Ridder, R.A. Hijmering, H. Akamatsu, L. Gottardi, J. Van der Kuur, J.-R. Gao , B.D. Jackson", this proc.